Numerical investigation of long-term operation of ground-source heat pumps at neighborhood level: Focus on thermal interactions and electricity consumption

Mohamad Ali Jaafar, Charles Maragna

Geothermics 96 (2021) 102172

Contents lists available at ScienceDirect

Geothermics

journal homepage: www.elsevier.com/locate/geothermics

Numerical investigation of long-term operation of ground-source heat pumps at neighborhood level: Focus on thermal interactions and electricity consumption

Mohamad Ali Jaafar, Charles Maragna *

BRGM (Geological and Mining Research Bureau), Geothermal department, 3 avenue Claude Guillemin, 45100 Orléans, France

ARTICLE INFO

Keywords:
Shallow geothermal energy
Ground-source heat pumps
Line source models
Long-term performance
Electrical consumption
Sustainable cities

ABSTRACT

A comprehensive numerical investigation of long-term operation of Ground-Sourced Heat Pumps through Borehole Heat Exchangers is presented. Thermal fluxes between systems are analyzed through a semi-analytical method based on line source models. Operation points of geothermal and backup systems are determined by an hourly-based non-linear constrained optimization. Simulations of a 12-buildings neighborhood demonstrated that middle-buildings experience higher electrical consumptions than corner-buildings. Thermal interactions could be interferences or synergies decreasing or increasing GSHP performances, respectively, depending mainly on heating/cooling balance. Parametrical study showed that low Darcy velocities, insulated ground surface, shorter heat-exchangers, and denser and compact neighborhoods enhance thermal interactions impacts.

1. Introduction

Renewable energies top the list of gainful solutions humans should widely apply to hold off climate change and global warming. One of these is geothermal energy, which is derived from the natural Earth's internal heat. Shallow geothermal energy targets geological formations at a typical temperature below 30°C to heat, cool and supply hot water for buildings. This is accomplished by means of Ground-Source Heat Pumps (GSHPs) through closed loop (vertical, horizontal, etc.) or open loop (aquifer heat pumps) systems (Mustafa Omer, 2008, Florides and Kalogirou, 2007).

Vertical closed loop systems, known as Borehole Heat Exchangers (BHEs), attract much attention since they are a scalable solution. However, BHEs need correct sizing and management to maintain their sustainability and avoid critical thermal changes in the underground. Modeling of BHE systems is a powerful tool to investigate their performance and sustainability, their technical potential, as well as their impacts on both the underground and neighboring systems. These investigations can therefore help energy decision makers to develop appropriately these systems and integrate them in sustainable energy plans.

The diversity of time and space scales involved in heat transfer around a BHE in operation makes the temperature prediction complex (Li and Lai, 2015). Numerical techniques can handle heterogeneous physical mechanisms at stake through finite-element (e.g. (Bauer et al., 2011; Carlini et al., 2016; Choi et al., 2011; Monzó et al., 2018; Tang and Nowamooz, 2018; Zanchini et al., 2012; Wołoszyn and Gołaś, 2013)), finite-difference (e.g. (Monzó et al., 2018; Lee and Lam, 2008; Mottaghy and Dijkshoorn, 2012)) or finite-volume approach (e.g. (Cai et al., 2019, Rees and He, 2013, Yavuzturk et al., 1999, Li and Zheng, 2009)). Despite that these methods are very accurate and agree well with experimental data (Carlini et al., 2016; Tang and Nowamooz, 2018; Cai et al., 2019; Li and Zheng, 2009), they suffer from long computational times which limit their application to specific cases with short simulation periods and space dimensions. In practice, they are barely able to study BHEs performance on the long term with short time steps (e.g. one hour).

Analytical approaches are useful alternatives since they are much less CPU-intensive. They rely on G-functions, i.e. non-dimensional thermal responses of the ground when unit-step heat pulse is applied on a BHE (Eskilson, 1987). Using these function, the evolution of temperature at any point of the underground is given by:

Abbreviations: COP, Coefficient of performance; SGE, Shallow geothermal energy; BHE, Borehole heat exchanger; ILSM, , Infinite line source model; FLSM, Finite line source model; GWF, Groundwater flow; MILSM, Moving infinite line source model; MFLSM, Moving finite line source model; GSHP, Ground-source heat pump; EH, Electrical heater; AHP, Air heat pump; HCF, Heat-carrier fluid.

* Corresponding author.
E-mail address: c.maragna@brgm.fr (C. Maragna).

https://doi.org/10.1016/j.geothermics.2021.102172
Received 15 February 2021; Received in revised form 22 April 2021; Accepted 10 June 2021
Available online 9 July 2021

Nomenclature

C_p	Specific heat capacity, J.kg^{-1}.K^{-1}
d	Distance, m
E	Energy, Wh
G	Thermal response, -
H	BHE Length, m
h	Ground surface Heat transfer coefficient, m^{-1}
k	Thermal conductivity, W.m^{-1}.K^{-1}
$\dot{m}_{nom}$	Mass flow rate, Kg.s^{-1}
P	Power, W
p	Linear power, W.m^{-1}
R	Thermal resistance, m.K.W^{-1}
r	Radius, m
T	Temperature, K
t	Time, s
v_D	Darcy velocity, m.s^{-1}
v_e	Effective heat transport velocity, m.s^{-1}
Greek symbols	
θ	Angle, °
α	Thermal diffusivity, $m^2.s^{-1}$
ρ	Density, $kg.m^{-3}$

Table 1
Main line source models for BHEs.

Model	Axial heat fluxes	Ground Water Flow (GWF)	References
Infinite Line Source (ILS)	No	No	(Carslaw and Jaeger, 1947)
Finite Line Source (FLS)	Yes	No	(Zeng et al., 2002)[23]
Moving Infinite Line Source (MILS)	No	Yes	(Diao et al., 2004)
Moving Finite Line Source (MFLS)	Yes	Yes	(Molina-Giraldo et al., 2011) (Rivera et al., 2015)[27]

$$\Delta T = T(x,y,z,t) - T_{gr} = \frac{p}{k_{gr}} G(x,y,z,t) \quad (1)$$

where T_{gr} represents the undisturbed temperature of the ground (K), p is the applied power by unit length (W.m^{-1}) and k_{gr} is the ground thermal conductivity (W.m^{-1}.K^{-1}).

These approaches assume an infinite homogeneous underground with a uniform initial temperature. They also deal separately with thermal processes in the inside and the outside regions of BHEs (Li and Lai, 2015, Koohi-Fayegh and Rosen, 2013). For the region between the BHE wall and the heat carrier fluid (HCF), a steady state heat transfer is usually assumed and a constant effective thermal resistance is used (Sharqawy et al., 2009, Lamarche et al., 2010). For the region between the BHE wall and the underground, it is described in time based on the line source theory, which offers an extremely attractive tool to simulate long-term behavior of BHEs (Li and Lai, 2015, Choi et al., 2011, Monzó et al., 2018, Lee and Lam, 2008, Rees and He, 2013). For instance, authors of (Choi et al., 2011) demonstrated that the high relative error against their 3D numerical model at first few hours decreases rapidly to less than 3% after around 50 hours. Multiple line source models have been proposed in the literature (Eskilson, 1987). These models and selected parameters are summarized in Table 1.

These models have been successfully applied to assess the technical potential of BHEs at large scales. This is determined based on thermal criteria of a tolerable maximum perturbation in the HCF (Casasso and Sethi, 2016, Miglani et al., 2018, Rivera et al., 2017) or in the subsurface temperature (García-Gil et al., 2015, Alcaraz et al., 2017). When multiple BHEs are installed, thermal interactions between them will be produced since they use the same underground resource (Kurevija et al., 2012). However, in most studies, for simplicity purposes, these interactions are either not taken into account (García-Gil et al., 2015, Casasso and Sethi, 2016) or avoided (Alcaraz et al., 2017, Zhang et al., 2015). Law and Dworkin (Law and Dworkin, 2016) have compared four types of buildings with different heating/cooling balances and different BHE configurations through a 3D finite element model in COMSOL Multiphysics. They concluded that thermal interactions are more important for compact configurations of BHE and unbalanced heat loads. Koohi-Fayegh et Rosen (Koohi-Fayegh and Rosen, 2014) have developed an analytical method based on the FLS model to study the effect of thermal interactions between two adjacent BHEs on the long-term performance of GSHPs. They considered ideal Heat Pump units to calculate the Coefficient of Performance (COP) of the installation. They concluded that the effect of thermal interactions on the COP depends on the cycle of the periodic thermal loads and the distance separating them. Thanks to the spatial superposition principle, Rivera et al. (Rivera et al., 2017) estimated the urban technical potential taking into account thermal interferences between adjacent systems. The purpose of their work was to study different degrees of thermal anomalies in the upper urban ground, known as subsurface urban heat islands (Bayer et al., 2019). However, the groundwater flow (GWF) is not taken into account and the investigations are not coupled with HP units. Miglani et al. (Miglani et al., 2018) overcome the second issue by comparing geothermal heat delivered to buildings and their heat demands. They spatially and temporally superimposed FLS solution to provide specific insights on the technical potential. They used an extra energy supply system for the unmet heat load by GSHPs. However, they also neglect the GWF in their model and roughly simulated HP units with a constant COP. In addition, they present results only for 10 years of operation while it is suggested to design and control BHEs for an operation period of at least 30 years (Kurevija et al., 2012). Li et al. (Li et al., 2015) coupled an ILS model for the underground temperature with a steady state model of HP units to study the performance of GSHPs during 15 years of operation for two buildings with square array BHEs. They concluded that the underground temperature may change significantly for large buildings and that the geothermal COP may be no more advantageous when the HCF temperature increase significantly during summer seasons.

These studies reveal that neglecting thermal interactions between systems may produce significant deviations from expected BHE thermal evolutions, especially in urban dense areas with unbalanced heat load. However, there is still a lack in understanding the effect of these interactions on GSHPs since HP units are oversimplified, i.e. they consider a constant COP for HP units, and the GWF set to zero. To overcome these limitations, the paper studies the long-term performance of neighboring BHE fields in dense urban areas based on semi-analytical models with hourly-based simulation (Section 2) to estimate the GSHP electrical and backup consumptions. One determines if the thermal interactions between the BHE fields are interferences or synergies based on the misbalance of energy injected into / extracted from the ground. The proposed model is validated with Feflow simulations (Section 3). Results are discussed in Section 4. A parameter analysis covers BHEs configuration, heating/cooling balance, boundary condition at the top surface and groundwater velocity (Section 5).

2. Model developments

In a preliminary phase, G-functions representative of every BHE fields and their interactions are computed based on line source models

and thermal resistance models. Hourly-time-step simulation over several years are then performed to determine temperature at each BHE field as well as GSHPs performance and backup consumption.

2.1. Input data and BHEs configurations

Every parcel is described by its dimensions and its hourly cooling and heating loads. BHEs are located in each field given the eligible area through an adaptation of the ASHRAE method (Bernier, 2006) to our problem, assuming identical BHEs with same length, see the Supporting Information. ASHRAE has been shown to be a useful and simple tool to design BHE fields (Fossa and Rolando, 2016). Moreover, HP units are characterized by their maximum calorific power, acceptable extreme temperatures of HCF and maps of COP. The underground is characterized by its initial temperature, thermal conductivity, heat capacity and groundwater velocity.

2.2. Thermal response of BHEs

Following assumptions are made:

(i) The underground is a semi-infinite medium with a uniform initial temperature.
(ii) The GWF is constant, horizontal and uniform according the depth.
(iii) Heat extraction rates are equal in BHEs of the same field and uniform along the depth of BHEs.
(iv) All BHEs are identical, having the same length and radius.
(v) Ambient temperature variation and geothermal gradient are not considered.
(vi) All physical properties are assumed to be constant and independent on temperature.

Self-G-functions (G_{Auto}) and G-functions between BHEs (G_{Inter}) are calculated over the whole simulation period. The BHE wall temperature is given by:

$$T_w(t) - T_{gr} = \frac{p}{k_{gr}} G_{Auto}(t) = \frac{P}{Hk_{gr}} G(t, r_w) \tag{2}$$

$G_{Inter(j,i)}$ represents the thermal response at the wall of a BHE i for a unit-step heat pulse applied on a BHE j. The wall temperature of the BHE i is then given by:

$$T_{w,i}(t) - T_{gr} = \frac{p_j}{k_{gr}} G_{Inter(j,i)}(t) = \frac{P_j}{Hk_{gr}} . G\left(t, d_{(i,j)}, \theta_{(i,j)}\right) \tag{3}$$

where $d_{(i,j)} = \sqrt{(x_i - x_j)^2 + (y_i - y_j)^2}$ is the distance between BHEs i and j; x_i, y_i, x_j and y_j their coordinates. $\theta_{(i,j)}$ is the angle between the line joining BHEs i to j and the GWF direction.

If there is no underground water flow, the Finite Line Source Model (FLSM) is used; otherwise the Moving Finite Line Source Model (MFLSM) is used. The G-functions account for three types of boundary conditions at the ground surface (GSBC): adiabatic, imposed temperature or mixed Cauchy-type. When there is no GWF, the solution of FLSM with an imposed temperature or an adiabatic condition at the top surface are given, respectively, by Eqs. (4) and (5) (Lamarche and Beauchamp, 2007):

$$G_{FLS}^{T_0}(t^*, \beta) = \frac{1}{2\pi}\left[\left(- D_A + \int_{\beta}^{\sqrt{\beta^2+1}} \frac{erfc(\omega z)}{\sqrt{z^2-\beta^2}} dz\right) - \left(D_B + \int_{\sqrt{\beta^2+1}}^{\sqrt{\beta^2+4}} \frac{erfc(\omega z)}{\sqrt{z^2-\beta^2}} dz\right)\right] \tag{4}$$

$$G_{FLS}^{\varnothing_0}(t^*, \beta) = \frac{1}{2\pi}\left[\left(- D_A + \int_{\beta}^{\sqrt{\beta^2+1}} \frac{erfc(\omega z)}{\sqrt{z^2-\beta^2}} dz\right) + \left(D_B + \int_{\sqrt{\beta^2+1}}^{\sqrt{\beta^2+4}} \frac{erfc(\omega z)}{\sqrt{z^2-\beta^2}} dz\right)\right] \tag{5}$$

where

$$D_A = \sqrt{\beta^2+1}\ \operatorname{erfc}\left(\omega\sqrt{\beta^2+1}\right) - \beta\operatorname{erfc}(\omega\beta) - \frac{(\exp(-\omega^2(\beta^2+1)) - \exp(-\omega^2\beta^2))}{\omega\sqrt{\pi}}$$

$$D_B = \sqrt{\beta^2+1}\ \operatorname{erfc}\left(\omega\sqrt{\beta^2+1}\right) - \frac{1}{2}\left(\beta\operatorname{erfc}(\omega\beta) + \sqrt{\beta^2+4}\ \operatorname{erfc}\left(\omega\sqrt{\beta^2+4}\right)\right) - \frac{\left(\exp(-\omega^2(\beta^2+1)) - \frac{1}{2}(\exp(-\omega^2\beta^2) + exp(-\omega^2(\beta^2+4)))\right)}{\omega\sqrt{\pi}}$$

$$\omega = \frac{H}{2\sqrt{\alpha_{gr}t}}, \alpha_{gr} = \left(\frac{k}{\rho Cp}\right)_{gr} \text{ and } \beta = \begin{cases} \frac{r_w}{H}, \text{ for } G_{Auto} \\ \frac{d_{(i,j)}}{H}, \text{ for } G_{Inter(j,i)} \end{cases}$$

Otherwise, when GWF is considered, MFLSM is used for both boundary conditions as follows (Molina-Giraldo et al., 2011):

$$G_{MFLS}^{T_0}(\beta,\omega,F_0,P_e) = \left(\frac{1}{2\pi}\right) g(P_e,\beta) \int_0^1 \left[\int_0^1 f(\omega,F_0,P_e) dz_1^* - \int_{-1}^0 f(\omega,F_0,P_e) dz_1^*\right] dz_2^* \tag{6}$$

$$G_{MFLS}^{\varnothing_0}(\beta,\omega,F_0,P_e) = \left(\frac{1}{2\pi}\right) g(P_e,\beta) \int_0^1 \left[\int_0^1 f(\omega,F_0,P_e) dz_1^* + \int_{-1}^0 f(\omega,F_0,P_e) dz_1^*\right] dz_2^* \tag{7}$$

Where:

$$g(P_e,\beta) = \begin{cases} I_0\left(\frac{P_e.\beta}{2}\right), for G_{Auto} \\ \exp\left[\frac{P_e}{2}\beta\right], \text{ for } G_{Inter(j,i)} \end{cases} \quad and \beta = \begin{cases} \frac{r_b}{H}, \text{ for } G_{Auto} \\ \frac{d_{(i,j)}}{H}\cos(\theta), \text{ for } G_{Inter(j,i)} \end{cases}$$

$$f(\omega,F_0,P_e) = \frac{1}{4\omega}\left[\exp\left(-\frac{P_e}{2}\omega\right) erfc\left(\frac{\omega - P_eF_0}{2\sqrt{F_0}}\right) + \exp\left(\frac{P_e}{2}\omega\right) erfc\left(\frac{\omega + P_eF_0}{2\sqrt{F_0}}\right)\right]$$

$$\omega = \begin{cases} \frac{1}{H}\sqrt{{r_b}^2 + (z_2 - z_1)^2}, \text{ for } G_{Auto} \\ \frac{1}{H}\sqrt{{d_{(i,j)}}^2 + (z_2 - z_1)^2}, \text{ for } G_{Inter(j,i)} \end{cases}$$

$z_1^* = \frac{z_1}{H}$ and $z_2^* = \frac{z_2}{H}$ normalized position along the emitter and receptor BHE respectively.

$F_0 = \frac{\alpha_{gr} t}{H^2}$ the Fourier number, $P_e = \frac{v_e H}{\alpha_{gr}}$ the Péclet number and $v_e = v_D \frac{(\rho C_p)_{gw}}{(\rho C_p)_{gr}}$where v_e and v_D are respectively the effective heat transport and Darcy velocities. α_{gr} represents the heat diffusivity of the underground. ρ *and* C_p represent respectively the density and the specific heat capacity. *gw* and *gr* stand for groundwater and the underground, respectively. To reduce computational times, these double integrals are transformed into simple integrals before implementation, see Appendix.

When a mixed Cauchy-type condition is considered, the solution for an imposed temperature is used and a contribution associated to a Cauchy-type boundary condition is added (Rivera et al., 2016):

$$G^h = G^{T_0} + \Delta G^h(\varepsilon, \beta, H, h) \tag{8}$$

Where:

$$\Delta G^h(\varepsilon,\beta,H,h) = \frac{1}{4\pi H h} g(P_e,\beta) \int_{\frac{r_b^2}{4\alpha_{gr} t}}^{\infty} \frac{1}{\varphi} exp\Bigg(- \varphi - \left(\frac{\varepsilon . v_e}{4\alpha_{gr}}\right)^2 \frac{1}{\varphi}\Bigg) \Psi(h,H,\varepsilon,\varphi) d\varphi$$

$$g(P_e,\beta) = \begin{cases} I_0\left(\frac{\beta . v_e}{2\alpha_{gr}}\right), \text{ for } G_{Auto} \\ exp\left[\frac{\beta . v_e}{2\alpha_{gr}}\right], \text{ for } G_{Inter(j,i)} \end{cases}$$

$$\Psi(h,H,\varepsilon,\varphi) = 2erf\left(\frac{H}{\varepsilon}\sqrt{\varphi}\right) - erf\left(\frac{2H}{\varepsilon}\sqrt{\varphi}\right) + exp\left[\left(\frac{h\varepsilon}{2}\right)^2 \frac{1}{\varphi}\right] \times \left[2exp(hH) erfc\left(\frac{H}{\varepsilon}\sqrt{\varphi} + \frac{h\varepsilon}{2\sqrt{\varphi}}\right) - erfc\left(\frac{h\varepsilon}{2\sqrt{\varphi}}\right) - exp(2hH) erfc\left(\frac{2H}{\varepsilon}\sqrt{\varphi} + \frac{h\varepsilon}{2\sqrt{\varphi}}\right)\right]$$

$$\beta = \begin{cases} \frac{r_b}{H}, \text{ for } G_{Auto} \\ \frac{d_{(i,j)}}{H} cos(\theta), \text{ for } G_{Inter(j,i)} \end{cases} \text{ and } \varepsilon = \begin{cases} r_b, \text{ for } G_{Auto} \\ d_{(i,j)}, \text{ for } G_{Inter(j,i)} \end{cases}$$

Since thermal demands vary naturally with time, heat extractions are regarded as a sum of pulse steps, and then thermal response at any time step n can be obtained by temporal superposition (Eskilson, 1987):

$$T^n - T_{gr} = \frac{1}{k_{gr}} \left\{ p^1 G^n + \sum_{l=1}^{n-1} \left(p^{l+1} - p^l\right) G^{n-l} \right\} \tag{9}$$

For the case of multiple BHEs, thermal interactions have to be taken into account. Combining G-functions (Eqs. (1-8) with spatial superposition principle (Eq. (9)), the temperature evolution of the wall of a BHE i for a configuration with Nb BHEs is described by:

$$T_{w\_i}^n - T_{gr} = \frac{1}{k_{gr}} \left[p_i^1 G_{Auto}^n + \sum_{l=1}^{n-1} \left(p_i^{l+1} - p_i^l\right) G_{Auto}^{n-l} \right] + \frac{1}{k_{gr}} \sum_{j \neq i}^{Nb} \left[p_j^1 G_{Inter(j,i)}^n + \sum_{l=1}^{n-1} \left(p_j^{l+1} - p_j^l\right) G_{Inter(j,i)}^{n-l} \right] \tag{10}$$

2.3. Mean temperature of HCF

Mean temperature of HCF is evaluated for each GSHP as the average of HCF temperatures of all BHEs connected to it. This means that all BHEs are assumed to be connected in parallel to the GSHP which is a common practice (Norme Suisse, 2010). For a GSHP I connected to Nb_I BHEs, the HCF temperature is then given by:

$$T_{f\_I}^n = \frac{1}{Nb\_I} \sum_{i \in I} T_{f\_i}^n \tag{11}$$

where $T_{f\_i}^n$ represents the HCF temperature of each BHE i connected to the GSHP I. Since spatial and temporal scales, characterizing the heat transfer within BHEs, are much smaller than those of the outside region (Li and Lai, 2015), and that we are interested only in the long term operation of GSHPs, the steady-state thermal resistance model is used to simulate the heat transfer between the borehole wall and the HCF, leading to:

$$T_{f\_i}^n = T_{w\_i}^n + R_b p_i^n \tag{12}$$

where R_b is the thermal resistance of BHEs (m.K.W^{-1}). Using assumption (iii), the HCF temperature of the GSHP I for a configuration with N GSHPs, each associated to a finite number of BHEs, is given by:

$$T_{f\_I}^n - T_{gr} = \frac{1}{k_{gr}} \sum_{J=1}^{N} \left\{ p_J^1 G_{(J,I)}^n + \sum_{l=1}^{n-1} \left(p_J^{l+1} - p_J^l\right) G_{(J,I)}^{n-l} \right\} \tag{13}$$

where

$$G_{(I,I)}^n = R_b k_{gr} + G_{Auto}^n + \frac{1}{Nb\_I} \sum_{i \in I} \sum_{\substack{j \in I \\ j \neq i}} G_{Inter(j,i)}^n \tag{14}$$

$$G_{(J,I)}^n = \frac{1}{Nb\_I} \sum_{i \in I} \sum_{j \in J} G_{Inter(j,i)}^n \tag{15}$$

2.4. Dynamical optimization problem

The operating point of every GSHP is determined by an hourly-based dynamic simulation. The problem at each time step is better formulated through a constrained non-linear optimization problem. Variables are BHE fields' injection temperature and their linear powers (i.e. applied powers by borehole length in the field). The variables vector is written as:

$$X^{tr} = \left[T_{fin\_1}^n,\ T_{fin\_2}^n,\ \ldots.,\ T_{fin\_N-1}^n,\ T_{fin\_N}^n,\ p_1^n,\ p_2^n,\ \ldots.,\ p_{N-1}^n,\ p_N^n \right] \tag{16}$$

Assuming that the HCF temperature is equal to the average between its inlet and outlet temperature (Eq. (17)), and a constant nominal mass flow rate in BHEs (Eq. (18)), injection temperature can be estimated by Eq. (19).

$$T_f = \frac{T_{fin} + T_{fout}}{2} \tag{17}$$

$$L.p = \dot{m}_{nom} . C_{p\_f} . \left(T_{fin} - T_{fout}\right) \tag{18}$$

$$T_{fin} = T_f + \frac{1}{2} . \frac{L.p}{\dot{m}_{nom} . C_{p\_f}} \tag{19}$$

where $\dot{m}_{nom}$ is the nominal mass flow rate (kg·s^{-1}), and C_{p_f} represents the specific heat capacity of the HCF (J·kg^{-1}·K^{-1}).The optimization problem is formulated in terms of geothermal fields inlet temperature rather than the mean one because geothermal regulations usually set tolerable limits on it. The objective function aims to maximize the use of geothermal energy (heat exchange with the underground):

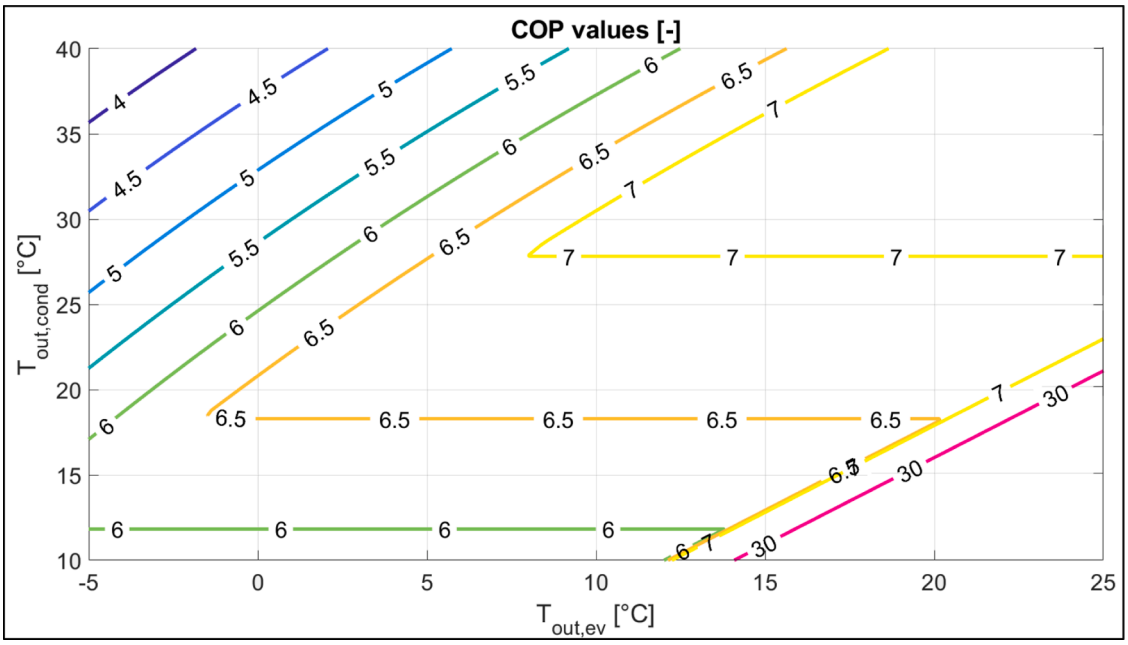

Fig. 1. COP as a function of evaporator and condenser outlet temperatures.

$$\max \sum_{I=1}^{N} \left| p_I^n \right| \tag{20}$$

This is set to ensure that geothermal energy is used as maximum as tolerated to cover buildings thermal demands.

This objective function is subject to multiple constraints. First kind is implemented through variables bounds. During cold seasons, heat is extracted from the underground and supplied into buildings. In addition, injection temperature of HCF is limited by a minimum value according to geothermal regulations. This can be expressed through bounds for each GSHP variables as follows:

$$T_{fin\_I}^n \geq T_{fin}^{min} \text{ and } p_I^n \leq 0 \tag{21}$$

Conversely, during hot seasons, heat is extracted from buildings and injected in the underground. Similarly, injection temperature of HCF is limited by a maximum value according to geothermal regulations:

$$T_{fin\_I}^n \leq T_{fin}^{max} \text{and} p_I^n > 0 \tag{22}$$

Every consumer is equipped with an electrical heater (EH) and an air heat pump (AHP) to cover heating and cooling demands respectively. When the GSHP does not fully cover thermal needs of buildings, these backup technologies are used to supply the rest. HCF temperatures and applied linear powers are coupled through G-functions. Since Eq. (13) is linear, it is implemented through linear equal constraints. For a system involving N GSHPs, this is expressed as follows:

$$A.X = b \tag{23}$$

where A is a matrix whose dimensions are $N \times (2N)$:

$$A = \begin{pmatrix} & & & & & & -G^1_{(1,1)} & -G^1_{(2,1)} & \cdots & & -G^1_{(i,1)} & \cdots & -G^1_{(N,1)} \\ k_{gr} & 0 & \cdots & \cdots & 0 & 0 & -G^1_{(1,2)} & -G^1_{(2,2)} & \cdots & & -G^1_{(i,2)} & \cdots & -G^1_{(N,2)} \\ 0 & k_{gr} & 0 & \cdots & \cdots\cdots & 0 & & & & & & & \\ \vdots & 0 & \ddots & 0 & \cdots\cdots & \vdots & \vdots & & \cdots & \ddots & \vdots & \cdots & \vdots \\ \vdots & \cdots\cdots & 0 & \ddots & 0 & \vdots & -G^1_{(i,1)} & \cdots & -G^1_{(N,1)} & -G^1_{(i,i)} & \cdots & -G^{1\ 1}_{(N,i)} & \\ 0 & \cdots\cdots & \cdots & 0 & k_{gr} & 0 & & & & & & & \\ 0 & 0 & \cdots & \cdots & 0 & k_{gr} & -G^1_{(i,2)} & \cdots & -G^1_{(N,2)} & \vdots & \ddots & \vdots & \cdots -G^1_{(N,N)} \\ & & & & & & \vdots & \cdots & \vdots & -G_{(i,N)} & & & \end{pmatrix} \tag{24}$$

and b is a vector whose length is N:

$$b = k_{gr}.T_{gr} + \begin{bmatrix} p^n_{conv\_1} \\ \vdots \\ p^n_{conv\_I} \\ \vdots \\ p^n_{conv\_N} \end{bmatrix} \tag{25}$$

where $p^n_{conv\_I}$ is the convoluted linear power applied on GSHP I on the time step n. It is expressed as:

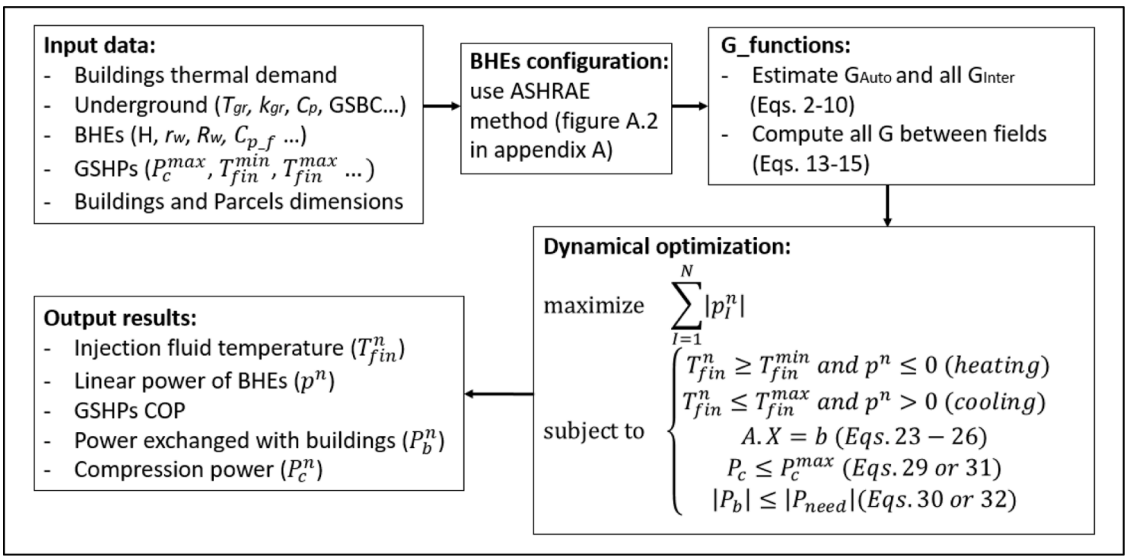

Fig. 2. Algorithm main steps.

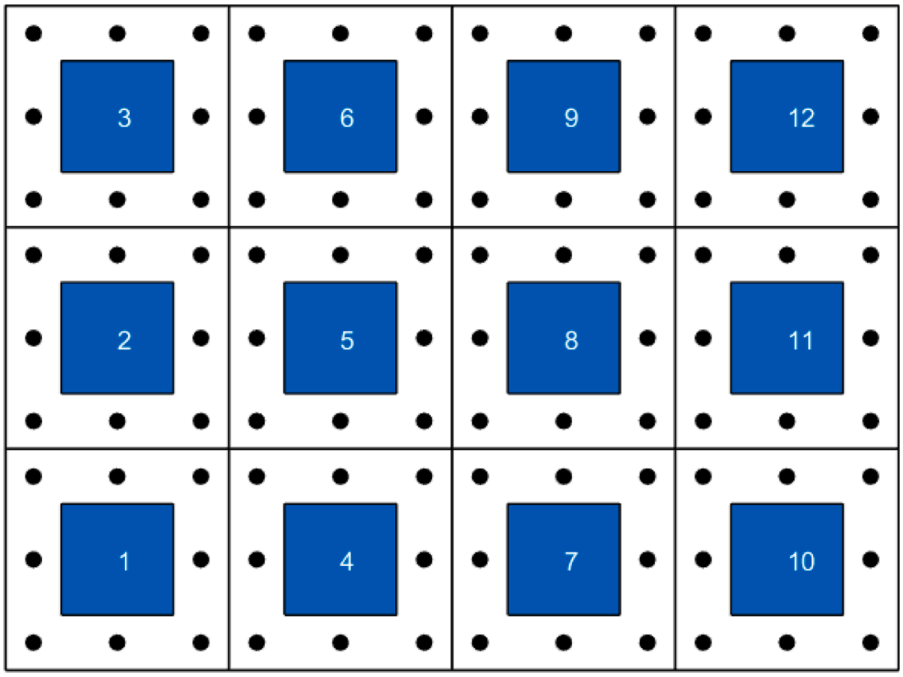

Fig. 3. Reference scheme of 4×3 parcels. The number of BHEs is the same for all parcels and equal to 8. BHEs are distributed homogeneously in the eligible area between parcels and buildings (in blue).

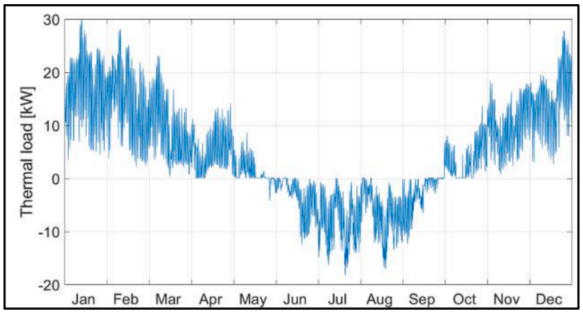

Fig. 4. Yearly thermal load of one consumer. Heating needs are positive, cooling needs are negative.

$$p_{conv\_I}^n = \sum_{J=1}^{N} \left\{ p_J^1 G_{(J,I)}^n - p_J^{n-1} G_{(J,I)}^1 + \sum_{l=1}^{n-2} \left(p_J^{l+1} - p_J^l\right) G_{(J,I)}^{n-l} \right\} \tag{26}$$

Finally, GSHPs powers are restricted by two conditions. The first is expressed through the compression power of each HP unit which cannot exceed its designed maximum compression power. The second is expressed through the heat extracted from/transferred to buildings which is limited by their thermal demand. They are respectively given in the followings:

$$P_c \leq P_c^{max} \tag{27}$$

$$|P_b| \leq |P_{need}| \tag{28}$$

Table 2
Main parameters in the case study.

Parameter	Reference Value	Unit
Underground specific heat capacity	2.4	$MJ{\cdot}K^{-1}{\cdot}m^{-3}$
Underground thermal conductivity	1.8	$W{\cdot}m^{-1}{\cdot}K^{-1}$
Underground undisturbed temperature	12.16	°C
BHE radius	8	cm
BHE thermal resistance	0.08	$K{\cdot}m{\cdot}W^{-1}$
BHE depth	100	m
Darcy velocity	0	m/y
Surface heat transfer coefficient	1	$W{\cdot}m^{-2}{\cdot}K^{-1}$
Parcels dimension	20	m
Buildings dimension	10	m
x-axis parcels number	4	-
y-axis parcels number	3	-
Minimal tolerable injection temperature	-3	°C
Maximal tolerable injection temperature	40	°C
Maximum heating power of GSHPs	30	kW
AHP COP	3.5	-
EH COP	1	-
Heating production temperature	35	°C
Cooling production temperature	17	°C
Simulation period	30	years

During cold seasons, Eqs. (27) and (28) yield:

$$\frac{p}{1-COP} \leq \frac{P_c^{max}}{L} \tag{29}$$

$$\frac{p.COP}{1-COP} \leq \frac{P_{need}}{L} \tag{30}$$

Similarly, during hot seasons, Eqs. (27) and (28) would be respectively like:

$$\frac{p}{COP} \leq \frac{P_c^{max}}{L} \tag{31}$$

$$p.\left(\frac{COP-1}{COP}\right) \leq \frac{P_{need}}{L} \tag{32}$$

The COP of HP units is calculated in terms of evaporator and condenser outlet temperatures $T_{ev,out}$ and $T_{cond,out}$ (see Fig. 1). Data originates from the technical documentation of the DYNACIAT LG-LGP model designed by the manufacturer CIAT. Note that if the BHE inlet temperature is low enough, geo-cooling is considered. Namely, if $T_{cond,out} < T_{ev,out}$ - 2°C, then the HP unit can be by-passed and the COP is set to an arbitrary high value (here COP = 30).

We assume that the production temperatures are constant for the heat transfer with buildings. Due to the non-linearity of COP expression, constraints (Eqs. (29-32)) are nonlinear.

2.5. Implementation and summary

All the above mentioned expressions are implemented in Matlab® environment. Constrained non-linear programming is solved with the fmincon function. To reduce computational times, G-functions are not computed on an hourly-time scale, but based on an aggregated logarithmic scale covering the whole simulation time and then interpolated, the relative error being below 0.1%. Convoluted powers between neighboring systems are weekly-updated (Eq. (26)), resulting in the root-mean-square error below 0.1°C. Summary of main steps is given in Fig. 2.

3. Model verification

The model was validated against a FEFLOW simulation with 3 BHE neighboring fields. An excellent agreement was found, the RMSE between temperatures simulated being in the range 1.4°C to 1.7°C. The results are presented in Section 1 of the supporting information.

4. Reference case study

The reference case study is a neighborhood of $4 \times 3 = 12$ identical buildings on identical 20 m wide square plots (cf. Fig. 3). Each plot is connected to 8 BHE; the sizing has been done with the ASHRAE method. The energy demand of each consumer is 53.9 MWh/y (30 kW) and 14.6 MWh/y (18.2 kW) for heating and cooling respectively (cf. Fig. 4). It has been modelled in the framework of the GRETA project (project, 2017) and concerns a well-insulated hotel in the city of Turin (Italy). The thermal loads have been reduced by 20% compared to original dataset. Main parameters are given in Table 2.

The results will be focused on consumers 5 and 12 since they have four and two immediate neighbors respectively and represent the worst and the best location in the neighborhood.

Fig. 5 represents the cumulated heating or cooling produced below a given temperature, e.g. the median temperature for heating production is around 7°C during the first year of operation for both BHE fields. The temperature then dramatically decreases over years. The cooling can then be produced for almost free via geocooling. However in heating mode, the BHE field inlet temperature often hits the -3°C threshold, resulting in a decreased delivered GSHP. The phenomena is more significate for GSHP 12 than GSHP 5 since it is located in the center of the neighborhood and is subject to the multiple interactions.

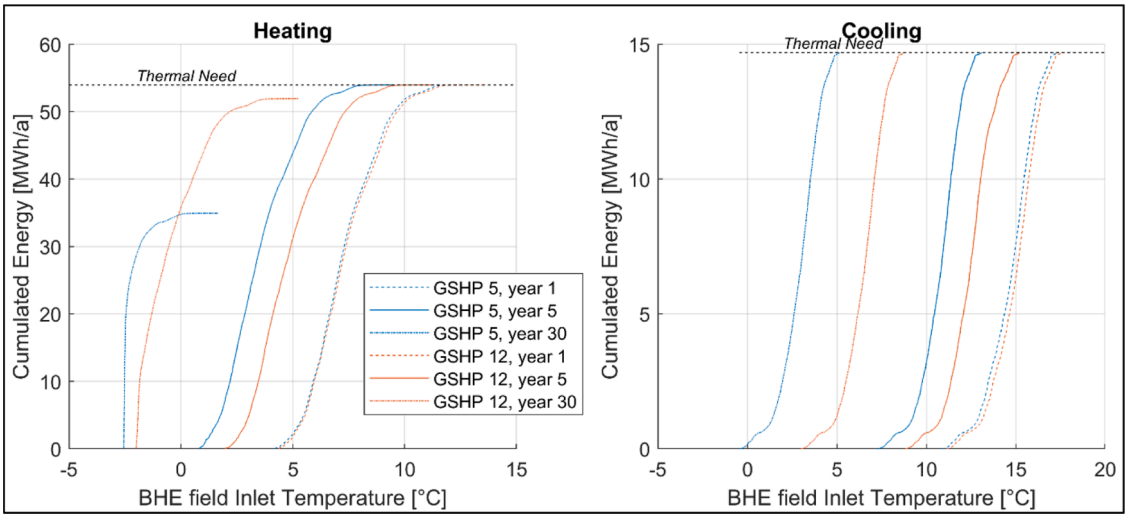

Fig. 5. Cumulated energy delivered by the GSHP for heating (left) and cooling (right) as a function of the BHE inlet temperature

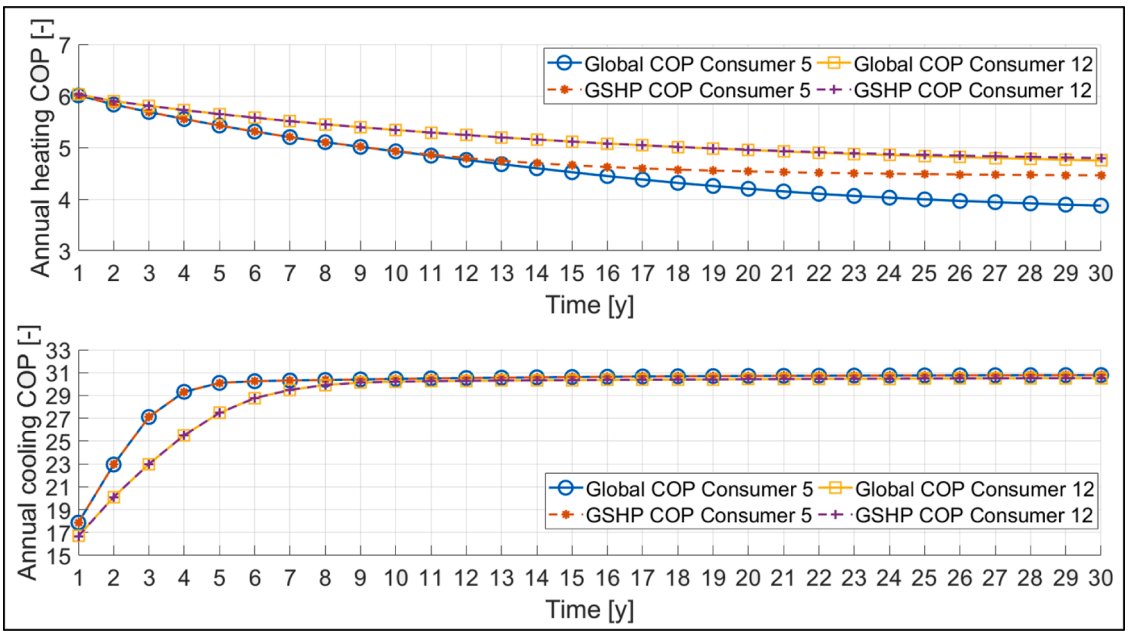

Fig. 6. Reference case: Yearly global and GSHP COP for heating (b1) and cooling (b2).

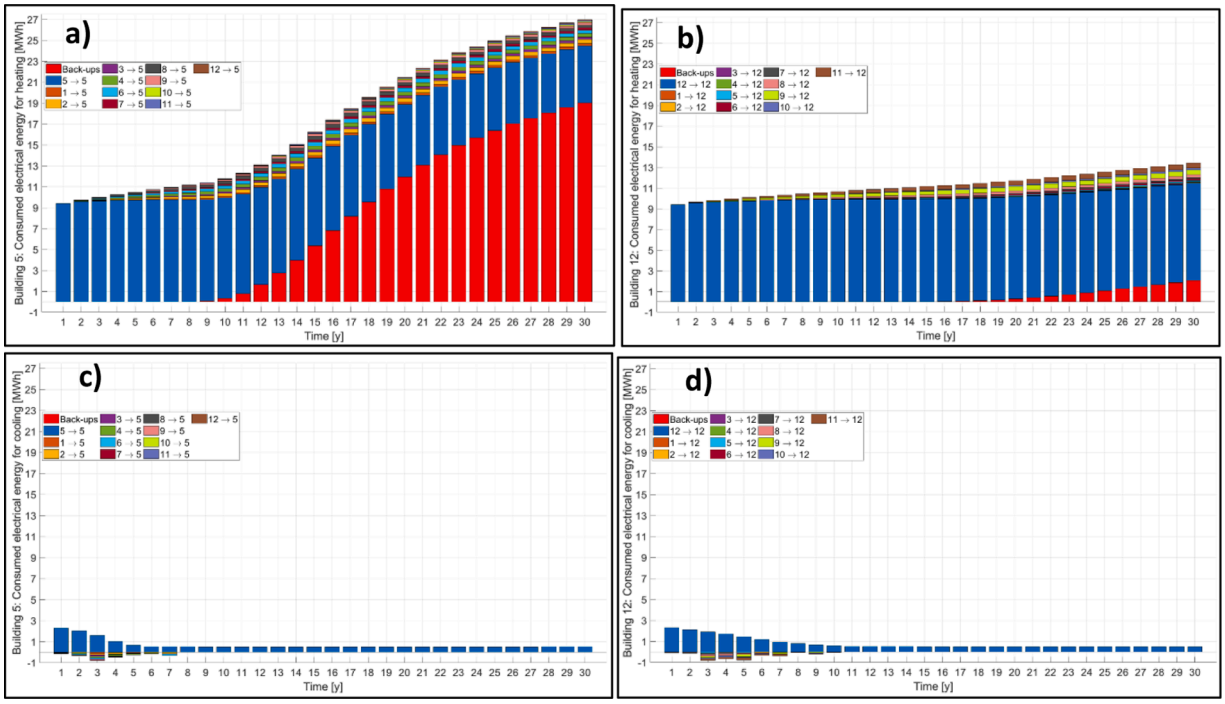

Fig. 7. Annual consumed electrical energy for a): building 5 in heating. b): building 12 in heating. c): building 5 in cooling and d): building 12 in cooling.

Table 3
Ranges considered in the parametric study.

Parameter	Reference Value	Range	Unit
Darcy velocity	0	0 to 70	$m \cdot y^{-1}$
Surface heat transfer coefficient	1	1 to 1000	$W \cdot m^{-2} \cdot K^{-1}$
BHE depth	100	50 to 200	m
Number of parcels in x-direction	4	2 to 12	-
Number of parcels in y-direction	3	1 to 6	-
Parcels dimension	20	15 to 35	m

Heating COPs of both consumers decrease in time during the whole operation time, especially for consumer 5 which is affected by the neighboring installations (cf. Fig. 6). Cooling COPs increase rapidly and then stabilize at an almost constant value due to the rapid decrease of the temperatures in both fields at the beginning of operations. Cooling COPs of consumer 5 is higher than cooling COP of consumer 12 since due to faster temperature decrease. It is worth reminding that EHs COP ($= 1$) is still much lower than GSHP COP even for the lowest values (≈ 4.3) obtained for worst last years of operation since the inlet temperature is

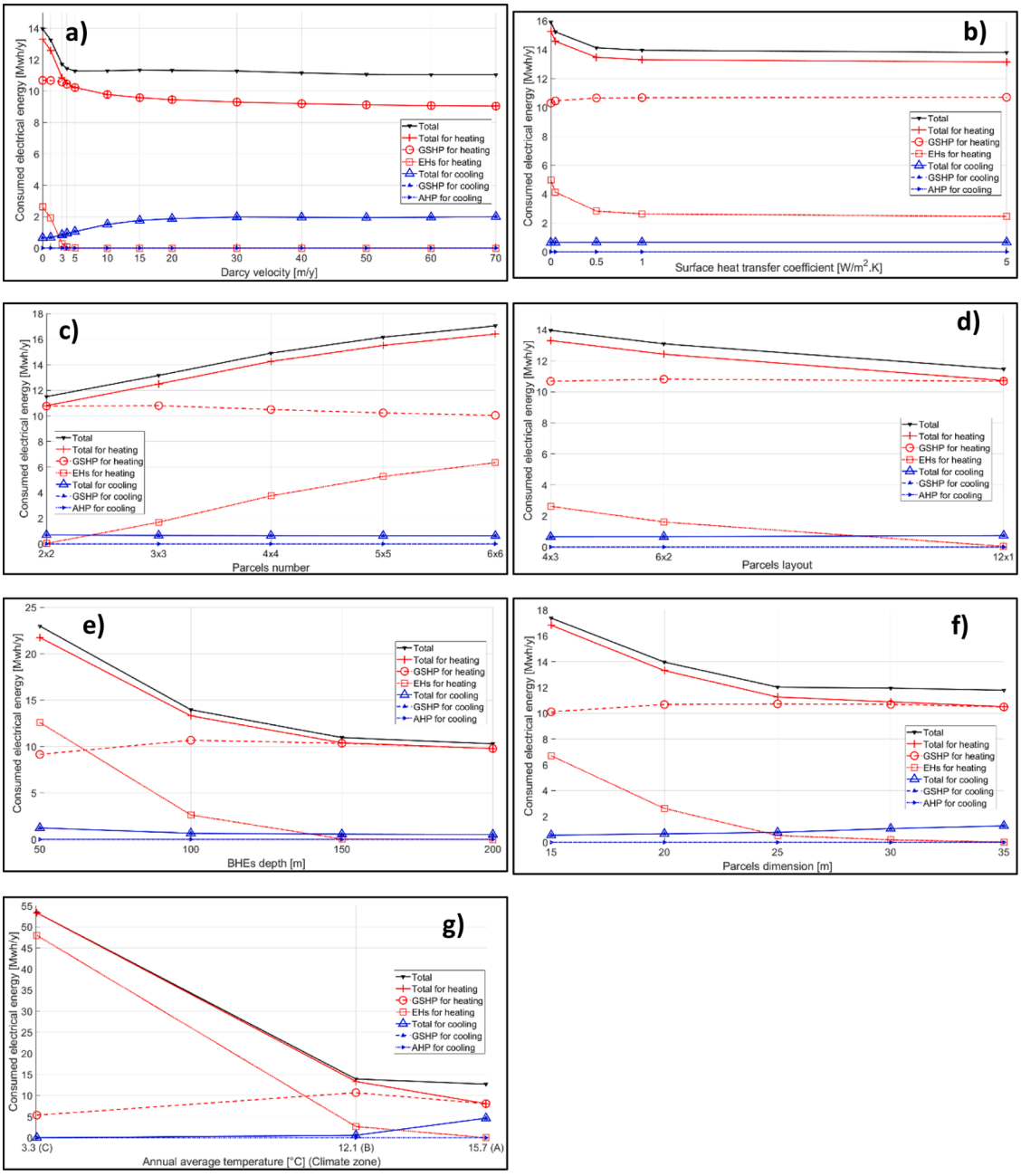

Fig. 8. Variation of the averaged electrical energy consumption for the 6 investigated parameters (a to f). The influence of the climate is represented through the annual average temperature (g).

Table 4
Considered number of boreholes when the parcel dimension varies.

Parcel dimension [m]	Number of BHEs [-]
15	9
20	8[(a)]
25	8
30	8
35	7

[(a)] : reference case

Table 5
Studied climate zones. Heating and cooling degree days are computed for a reference temperature of 18°C.

Climate zone	City	Average annual temperature [°C]	Heating degree days	Cooling degree days
A	Genoa	15.76	1375	558
B	Turin	12.16	2453	322[(a)]
C	Davos	3.33	5356	0

[(a)] reference case

not allowed to go under the lower limit set to -3°C. One may be interested to further estimate the contribution of neighboring installations to the COP of a given installation. A "what-if" electrical consumption of the installation, if it was far away from other installations, is computed. The spatial superimposition principles allows to estimate the temperature changes from every BHE field. The hourly contribution of K in the electrical consumption of I is determined by the difference between the real electrical power of I and a modified one (obtained for the same

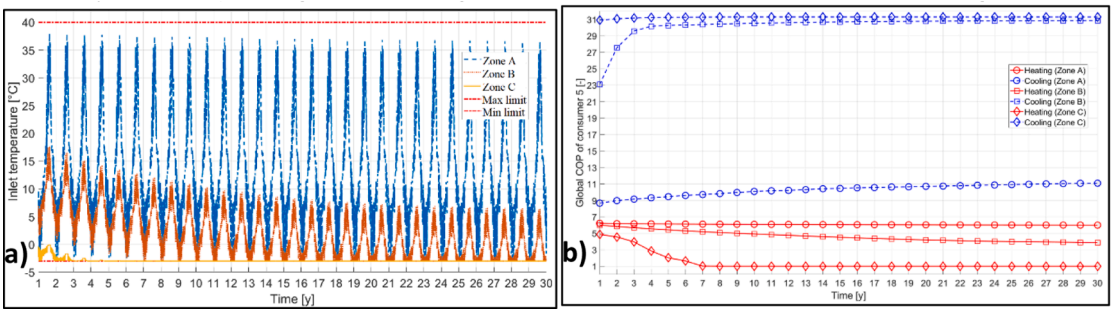

Fig. 9. Influence of the three climate zones on central BHE field (i.e. installation 5): a) Evolution of the inlet temperature into the BHE field. b) Annual global COP for heating and cooling purposes.

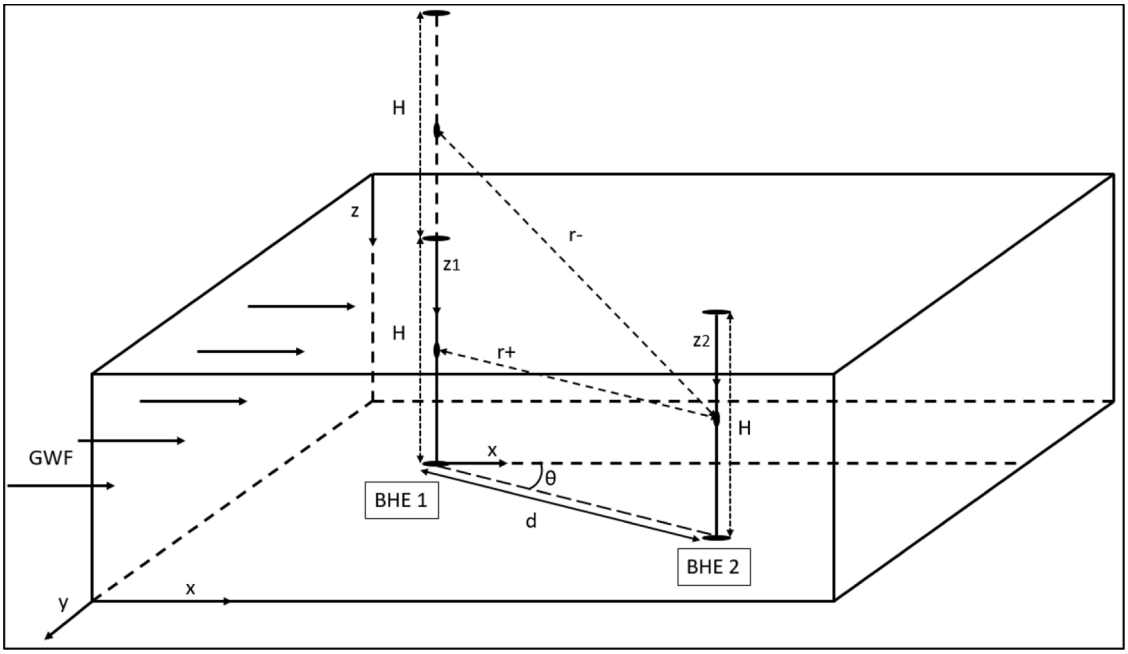

Fig. B.1. Schematic showing two boreholes. Power is applied on BHE 1.

power provided to/extracted from building with a modified fluid temperature). This modified fluid temperature is calculated by neglecting the effect of the field K:

$$T_{f\_I}^{n-modified} - T_{gr} = \frac{1}{k_{gr}} \sum_{J \neq K}^{N} \left\{ p_J^1 G_{(J,I)}^n + \sum_{l=1}^{n-1} \left(p_J^{l+1} - p_J^l \right) G_{(J,I)}^{n-l} \right\} \tag{33}$$

$$COP_I^{n-modified} = \begin{cases} COP\left(T_{fin\_I}^{n-modified}, T_{heat}^{prod}\right), & Heating\ mode \\ COP\left(T_{cool}^{prod}, T_{fin\_I}^{n-modified}\right), & Cooling\ mode \end{cases} \tag{34}$$

$$Cont_{K \to I}^n = \begin{cases} P_{c-I}^n - \dfrac{|P_b^n|}{COP_I^{n-modified}}, & Heating\ mode \\ P_{c-I}^n - \dfrac{|P_b|}{COP_I^{n-modified} - 1}, & Cooling\ mode \end{cases} \tag{35}$$

Indeed, due to the misbalance of the thermal flux on the ground, only the cooling benefits from synergies, see Fig. 7, where positive (resp. negative) bar values mean that the field K increases and (resp. decreases) the electrical consumption of the GSHP of consumer I, and that the interaction is a disturbance (resp. a synergy).

5. Parametric study

A parametric study has been carried out by varying 6 parameters around the reference values (cf. Table 3), as well as the climate zone. The parameters have been varied once at a time, i.e. the influence of coupled variations have not been investigated. The electrical consumption averaged on the 12 consumers is reported in Fig. 8. Note that regional flow, if any, follows the horizontal axis from the left to the right in Fig. 3. Note also that the number of borehole has been changed when the parcel dimension has been changed (cf. Table 4).

Three climates and associated load curves produced in the framework of the GRETA project have been considered (project, 2017). They represent extreme cases according to the balance between heating and cooling demands (climates A and C, see Table 5 and Fig. 9).

The following interpretations can be drawn:

- Effect of the underground water flow: No matter the Darcy velocity magnitude, heating electrical consumption remains much higher than cooling one (cf. Fig. 8a). Faster underground flows decrease total energy consumed for heating and increase total energy consumed for cooling. The total consumed energy decreases rapidly between 0 and 5 m/y, and then remains stable. As Darcy velocity increases, the cooling storage effect is taken away by advection fluxes due to the

regional flow, which makes geothermal cooling more expensive and heating cheaper.

- Effect of the top boundary condition: The increase of heat transfer coefficient h leads to the increase of the underground temperature due to the discharge of the "stored cold" by the top surface (cf. Fig. 8b). Note that only values of h up to 5 $W{\cdot}m^{-2}{\cdot}K^{-1}$ are represented since an asymptotic value was reached. The reference value of 1 $W{\cdot}m^{-2}{\cdot}K^{-1}$ gives results very close to the Dirichlet-type top boundary condition. The reported line source models often consider a Dirichlet-type top boundary condition (i.e. h $\rightarrow\infty$)., i.e. a constant temperature imposed at the surface. This points out that the top boundary condition must be selected with care given the local conditions.
- Effect of parcels number: A square arrangement of buildings has been considered, from 2×2 to 6×6. When the parcels number increases, electrical consumption of buildings slightly decreases for cooling but significantly increases for heating (cf. Fig. 8c, where the reference case being 2×3 is not represented). Indeed, the installations located in the heart of the neighborhood get more and more impacted by the cold injected into the ground by the BHE fields in the neighborhood periphery.
- Effect of parcels layout: Stretched layouts significantly decrease the total electricity consumed for heating, while slightly increases the electricity consumed for cooling (cf. Fig. 8d), since the excess cold injected into the ground can better diffuse beyond the neighborhood. Note that the number of parcels remains 12.
- Effect of BHEs depth: In order to get comparable results, all cases are designed with 8 100 m deep BHEs, as for the reference case. As BHE gets deeper, so that the volume of soil being solicited increases, the overall electricity consumption decreases (cf. Fig. 8e). It is worth to remark that the gain is not proportional to the BHE depth, the marginal gain decreases with deeper BHE.
- Effect of parcels dimension: BHEs fields do not have the same configuration for all cases, since the ASHRAE method depends on parcels dimension. The number of BHEs per field are provided in Table 4, with smaller number of BHE per field for larger parcels. The backup energy for heating drastically decreased for 25 m, and completely vanishes at 35 m (cf. Fig. 8f). A dimension of 35 m is enough, for the studied case, to avoid injection temperature to drop below the lower imposed limit (-3°C).

6. Conclusions

A semi-analytical method is proposed to study the long-term performance of hybrid GSHPs connected to BHE fields at neighborhood level. It is based on line source models. The method determines operation points of GSHPs based on an hourly-time-step constrained nonlinear programming, assuming variable COP of GSHPs. It allows investigating thermal interactions between BHEs fields by estimating energetics fluxes between BHEs fields and the impact on their electrical consumptions.

Geothermal operation of a neighborhood of 12 identical buildings was studied over 30 years of heating-dominated thermal load. The central consumer needs much more backup heaters to complete its heating demand compared to the corner consumer. Thermal interactions could be interferences or synergies and depend strongly on time and distances between geothermal fields. Finally, the crucial role of thermal interactions to forecast the backup consumption has been demonstrated.

The present work highlights the importance of taking into account thermal interactions between systems especially for compact and big neighborhoods to accurately expect operation costs in terms of both geothermal systems and backup technologies for heating and cooling supply. It also pinpoints the most influencing parameters and how they affect the geothermal operation. Modeling of backup systems showed advantages of integrating SGE in energy planning of cities by saving a lot of operation costs in most cases. However, since the proposed method is based on analytical models, the present method has some limitations especially in really produce different layers of the underground and the complex shape of the GWF. On the other hand, it shows the usefulness of these analytical models to precisely investigate effects of the governed parameters on the operation of geothermal systems in a relatively short computational time compared to numerical software. Upcoming works will be interested in overcoming limitations of analytical models and also on the other hand to integrate open-loop geothermal systems in the energy planning of sustainable cities.

Author statement

Mohamad Ali Jaafar: Conceptualization, Data curation, Formal analysis, Investigation, Methodology, Software, Supervision, Validation, Visualization, Roles/Writing - original draft, Writing - review & editing

Charles Maragna: Funding acquisition, Methodology, Project administration, Software, Supervision, Validation, Writing - review & editing

Declaration of Competing Interest

The authors declare that they have no known competing financial interests or personal relationships that could have appeared to influence the work reported in this paper.

Acknowledgments

This work was supported by the French National Agency for Research (ANR) under grant agreement 16-CARN-003-01, REDEEM action.

Supplementary materials

Supplementary material associated with this article can be found, in the online version, at doi:10.1016/j.geothermics.2021.102172.

Appendix. Alternative formulation of the Moving Finite Line Source Model

The purpose herein is to transform double integrals of the MFLSM into simple integrals which need less computational time to be resolved. The method followed is similar to the one proposed in (Lamarche and Beauchamp, 2007) for the FLSM (See Fig. B.1). The general solution of MFLSM is given by the following:

$$G_{MFLS}(d^*,\theta,F_0,P_e)=\left(\frac{1}{2\pi}\right)exp\left[\frac{P_e}{2}d^*cos(\theta)\right]\left[(I_1+I_2)\pm(I_3+I_4)\right] \quad (B.1)$$

In Eq. (B.1), "±" reads " + " for an adiabatic condition at the top surface and " − " for a top surface with an imposed initial temperature, and:

$$I_1 = \frac{1}{4}\int_0^1\int_0^1 \frac{1}{r_+^*}\exp\left(-\frac{P_e}{2}r_+^*\right) erfc\left(\frac{r_+^* - P_eF_0}{2\sqrt{F_0}}\right) dz_2^* dz_1^*$$

$$I_2 = \frac{1}{4}\int_0^1\int_0^1 \frac{1}{r_+^*}\exp\left(+\frac{P_e}{2}r_+^*\right) erfc\left(\frac{r_+^* + P_eF_0}{2\sqrt{F_0}}\right) dz_2^* dz_1^*$$

$$I_3 = \frac{1}{4}\int_0^1\int_0^1 \frac{1}{r_-^*}\exp\left(-\frac{P_e}{2}r_-^*\right) erfc\left(\frac{r_-^* - P_eF_0}{2\sqrt{F_0}}\right) dz_2^* dz_1^*$$

$$I_4 = \frac{1}{4}\int_0^1\int_0^1 \frac{1}{r_-^*}\exp\left(+\frac{P_e}{2}r_+^*\right) erfc\left(\frac{r_-^* + P_eF_0}{2\sqrt{F_0}}\right) dz_2^* dz_1^*$$

$$r_-^* = \sqrt{d^{*2} + (z_2^* + z_1^*)^2}, r_+^* = \sqrt{d^{*2} + (z_2^* - z_1^*)^2} \text{ and } d^* = \frac{d_{(i,j)}}{H}$$

In order to resolve I_1 the interval of the second integral is divided as follows:

$$I_1 = \frac{1}{4}(I_{11} + I_{12}) = \frac{1}{4}\left(\int_0^1\int_0^{z_2^*} \frac{1}{r_+^*}\exp\left(-\frac{P_e}{2}r_+^*\right) erfc\left(\frac{r_+^* - P_eF_0}{2\sqrt{F_0}}\right) dz_2^* dz_1^* + \int_0^1\int_{z_2^*}^1 \frac{1}{r_+^*}\exp\left(-\frac{P_e}{2}r_+^*\right) erfc\left(\frac{r_+^* - P_eF_0}{2\sqrt{F_0}}\right) dz_2^* dz_1^*\right) \quad (B.2)$$

Since that $r_+^* = \sqrt{d^{*2} + (z_2^* - z_1^*)^2}$ and for I_{11}, $z_1^* < z_2^*$, it is obtained that $z_2^* - z_1^* = \sqrt{r_+^{*2} - d^{*2}}$ and $dz_1^* = \frac{-r_+^*}{\sqrt{r_+^{*2} - d^{*2}}} dr_+^*$. If the variable change is applied to I_{11}, it would be like:

$$I_{11} = \int_0^1 \int_{d^*}^{\sqrt{d^{*2} + z_2^{*2}}} \exp\left(-\frac{P_e}{2}r_+^*\right) erfc\left(\frac{r_+^* - P_eF_0}{2\sqrt{F_0}}\right) \frac{1}{\sqrt{r_+^{*2} - d^{*2}}} dz_2^* dr_+^* \quad (B.3)$$

Since the inner expression depends only on r_+^* and by inverting the integration sign, I_{11} would be equivalent to the following integral:

$$I_{11} = \int_{\sqrt{r_+^{*2} - d^{*2}}}^1 \int_{d^*}^{\sqrt{d^{*2}+1}} \exp\left(-\frac{P_e}{2}r_+^*\right) erfc\left(\frac{r_+^* - P_eF_0}{2\sqrt{F_0}}\right) \frac{1}{\sqrt{r_+^{*2} - d^{*2}}} dz_2^* dr_+^* = \int_{d^*}^{\sqrt{d^{*2}+1}} \exp\left(-\frac{P_e}{2}r_+^*\right) erfc\left(\frac{r_+^* - P_eF_0}{2\sqrt{F_0}}\right)\left(\frac{1}{\sqrt{r_+^{*2} - d^{*2}}} - 1\right) dr_+^* \quad (B.4)$$

By following the same procedure for the integral I_{12}, for which $z_1^* > z_2^*$, it can be shown that it is equivalent to I_{11}, which implies that $I_1 = \frac{1}{2}I_{11}$. By dividing also I_2 into I_{21} and I_{22} and following the same procedure (the variable change and the integration sign invert):

$$I_2 = \frac{1}{4}(I_{21} + I_{22}) = \frac{1}{2}I_{21} = \frac{1}{2}\left[\int_{d^*}^{\sqrt{d^{*2}+1}} \exp\left(\frac{P_e}{2}r_+^*\right) erfc\left(\frac{r_+^* + P_eF_0}{2\sqrt{F_0}}\right)\left(\frac{1}{\sqrt{r_+^{*2} - d^{*2}}} - 1\right) dr_+^*\right] \quad (B.5)$$

A similar procedure is used to transform I_3 and I_4 to simple integrals for which $r_-^* = \sqrt{d^{*2} + (z_2^* + z_1^*)^2}$ is employed. They are respectively equivalent to the following expressions:

$$I_3 = \frac{1}{4}\left[\int_{d^*}^{\sqrt{d^{*2}+1}} \exp\left(-\frac{P_e}{2}r_-^*\right) erfc\left(\frac{r_-^* - P_eF_0}{2\sqrt{F_0}}\right) dr_-^* + \int_{\sqrt{d^{*2}+1}}^{\sqrt{d^{*2}+4}} \exp\left(-\frac{P_e}{2}r_-^*\right) erfc\left(\frac{r_-^* - P_eF_0}{2\sqrt{F_0}}\right)\left(\frac{2}{\sqrt{r_-^{*2} - d^{*2}}} - 1\right) dr_-^*\right] \quad (B.6)$$

$$I_4 = \frac{1}{4}\left[\int_{d^*}^{\sqrt{d^{*2}+1}} \exp\left(\frac{P_e}{2}r_-^*\right) erfc\left(\frac{r_-^* + P_eF_0}{2\sqrt{F_0}}\right) dr_-^* + \int_{\sqrt{d^{*2}+1}}^{\sqrt{d^{*2}+4}} \exp\left(\frac{P_e}{2}r_-^*\right) erfc\left(\frac{r_-^* + P_eF_0}{2\sqrt{F_0}}\right)\left(\frac{2}{\sqrt{r_-^{*2} - d^{*2}}} - 1\right) dr_-^*\right] \quad (B.7)$$

The Supporting Information reports the validation of these equations.

References

Mustafa Omer, A., 2008. Ground-source heat pumps systems and applications. Renew. Sustain. Energy Rev. 12, 344–371. https://doi.org/10.1016/j.rser.2006.10.003.

Florides, G., Kalogirou, S., 2007. Ground heat exchangers-A review of systems, models and applications. Renew. Energy 32, 2461–2478. https://doi.org/10.1016/j.renene.2006.12.014.

Li, M., Lai, A.C.K., 2015. Review of analytical models for heat transfer by vertical ground heat exchangers (GHEs): a perspective of time and space scales. Appl. Energy. https://doi.org/10.1016/j.apenergy.2015.04.070.

Bauer, D., Heidemann, W., Diersch, H.J.G., 2011. Transient 3D analysis of borehole heat exchanger modeling. Geothermics. https://doi.org/10.1016/j.geothermics.2011.08.001.

Carlini, M., Allegrini, E., Castellucci, S., 2016. Numerical Simulation of a Down-hole Heat Exchanger: an Application to a Case Study in Central Italy. Energy Procedia 101, 512–519. https://doi.org/10.1016/j.egypro.2016.11.065.

Choi, J.C., Lee, S.R., Lee, D.S., 2011. Numerical simulation of vertical ground heat exchangers: intermittent operation in unsaturated soil conditions. Comput. Geotech. 38, 949–958. https://doi.org/10.1016/j.compgeo.2011.07.004.
Monzó, P., Puttige, A.R., Acuña, J., Mogensen, P., Cazorla, A., Rodriguez, J., et al., 2018. Numerical modeling of ground thermal response with borehole heat exchangers connected in parallel. Energy Build. 172, 371–384. https://doi.org/10.1016/j.enbuild.2018.04.057.
Tang, F., Nowamooz, H., 2018. Long-term performance of a shallow borehole heat exchanger installed in a geothermal field of Alsace region. Renew. Energy 128, 210–222. https://doi.org/10.1016/j.renene.2018.05.073.
Zanchini, E., Lazzari, S., Priarone, A., 2012. Long-term performance of large borehole heat exchanger fields with unbalanced seasonal loads and groundwater flow. Energy 38, 66–77. https://doi.org/10.1016/j.energy.2011.12.038.
Wołoszyn, J., Gołaś, A., 2013. Modelling of a borehole heat exchanger using a finite element with multiple degrees of freedom. Geothermics 47, 13–26. https://doi.org/10.1016/j.geothermics.2013.01.002.
Lee, C.K., Lam, H.N., 2008. Computer simulation of borehole ground heat exchangers for geothermal heat pump systems. Renew. Energy 33, 1286–1296. https://doi.org/10.1016/j.renene.2007.07.006.
Mottaghy, D., Dijkshoorn, L., 2012. Implementing an effective finite difference formulation for borehole heat exchangers into a heat and mass transport code. Renew. Energy 45, 59–71. https://doi.org/10.1016/j.renene.2012.02.013.
Cai, W., Wang, F., Liu, J., Wang, Z., Ma, Z., 2019. Experimental and numerical investigation of heat transfer performance and sustainability of deep borehole heat exchangers coupled with ground source heat pump systems. Appl. Therm. Eng. 149, 975–986. https://doi.org/10.1016/j.applthermaleng.2018.12.094.
Rees, S.J., He, M., 2013. A three-dimensional numerical model of borehole heat exchanger heat transfer and fluid flow. Geothermics 46, 1–13. https://doi.org/10.1016/j.geothermics.2012.10.004.
Yavuzturk, C., Spitler, J.D., Rees, S.J., 1999. A Transient two-dimensional finite volume model for the simulation of vertical U-tube ground heat exchangers. ASHRAE Trans. 105, 465–474.
Li, Z., Zheng, M., 2009. Development of a numerical model for the simulation of vertical U-tube ground heat exchangers. Appl. Therm. Eng. 29, 920–924. https://doi.org/10.1016/j.applthermaleng.2008.04.024.
Eskilson, P. Thermal analysis of heat extraction boreholes. 1987.
Koohi-Fayegh, S., Rosen, MA., 2013. A review of the modelling of thermally interacting multiple boreholes. Sustain 5, 2519–2536. https://doi.org/10.3390/su5062519.
Sharqawy, M.H., Mokheimer, E.M., Badr, H.M., 2009. Effective pipe-to-borehole thermal resistance for vertical ground heat exchangers. Geothermics 38, 271–277. https://doi.org/10.1016/j.geothermics.2009.02.001.
Lamarche, L., Kajl, S., Beauchamp, B., 2010. A review of methods to evaluate borehole thermal resistances in geothermal heat-pump systems. Geothermics. https://doi.org/10.1016/j.geothermics.2010.03.003.
Carslaw, H.S., Jaeger, J.C. Conduction of Heat in Solids. Oxford: 1947.
Zeng, H.Y., Diao, N.R., Fang, Z.H., 2002. A finite line-source model for boreholes in geothermal heat exchangers. Heat Transf. - Asian Res. 31, 558–567. https://doi.org/10.1002/htj.10057.
Lamarche, L., Beauchamp, B., 2007. A new contribution to the finite line-source model for geothermal boreholes. Energy Build. https://doi.org/10.1016/j.enbuild.2006.06.003.
Diao, N., Li, Q., Fang, Z., 2004. Heat transfer in ground heat exchangers with groundwater advection. Int. J. Therm. Sci. 43, 1203–1211. https://doi.org/10.1016/j.ijthermalsci.2004.04.009.
Molina-Giraldo, N., Blum, P., Zhu, K., Bayer, P., Fang, Z., 2011. A moving finite line source model to simulate borehole heat exchangers with groundwater advection. Int. J. Therm. Sci. 50, 2506–2513. https://doi.org/10.1016/j.ijthermalsci.2011.06.012.
Rivera, J.A., Blum, P., Bayer, P., 2015. Analytical simulation of groundwater flow and land surface effects on thermal plumes of borehole heat exchangers. Appl. Energy. https://doi.org/10.1016/j.apenergy.2015.02.035.
Rivera, J.A., Blum, P., Bayer, P., 2016. A finite line source model with Cauchy-type top boundary conditions for simulating near surface effects on borehole heat exchangers. Energy 98, 50–63. https://doi.org/10.1016/j.energy.2015.12.129.
Casasso, A., Sethi, R.G., 2016. POT: a quantitative method for the assessment and mapping of the shallow geothermal potential. Energy 106, 765–773. https://doi.org/10.1016/j.energy.2016.03.091.
Miglani, S., Orehounig, K., Carmeliet, J., 2018. A methodology to calculate long-term shallow geothermal energy potential for an urban neighbourhood. Energy Build. 159, 462–473. https://doi.org/10.1016/j.enbuild.2017.10.100.
Rivera, J.A., Blum, P., Bayer, P., 2017. Increased ground temperatures in urban areas: Estimation of the technical geothermal potential. Renew. Energy 103, 388–400. https://doi.org/10.1016/j.renene.2016.11.005.
García-Gil, A., Vázquez-Suñe, E., Alcaraz, M.M., Juan, A.S., Sánchez-Navarro, J.Á., Montlleó, M., et al., 2015. GIS-supported mapping of low-temperature geothermal potential taking groundwater flow into account. Renew. Energy 77, 268–278. https://doi.org/10.1016/j.renene.2014.11.096.
Alcaraz, M., Vives, L., Vázquez-Suñé, E., 2017. The T-I-GERmethod: a graphical alternative to support the design and management of shallow geothermal energy exploitations at the metropolitan scale. Renew. Energy 109, 213–221. https://doi.org/10.1016/j.renene.2017.03.022.
Kurevija, T., Vulin, D., Krapec, V., 2012. Effect of borehole array geometry and thermal interferences on geothermal heat pump system. Energy Convers. Manag. 60, 134–142. https://doi.org/10.1016/j.enconman.2012.02.012.
Zhang, Y., Choudhary, R., Soga, K., 2015. Influence of GSHP system design parameters on the geothermal application capacity and electricity consumption at city-scale for Westminster, London. Energy Build. 106, 3–12. https://doi.org/10.1016/j.enbuild.2015.07.065.
Law, Y.L.E., Dworkin, S.B., 2016. Characterization of the effects of borehole configuration and interference with long term ground temperature modelling of ground source heat pumps. Appl. Energy 179, 1032–1047. https://doi.org/10.1016/j.apenergy.2016.07.048.
Koohi-Fayegh, S., Rosen, M.A., 2014. An analytical approach to evaluating the effect of thermal interaction of geothermal heat exchangers on ground heat pump efficiency. Energy Convers. Manag. 78, 184–192. https://doi.org/10.1016/j.enconman.2013.09.064.
Bayer, P., Attard, G., Blum, P., Menberg, K., 2019. The geothermal potential of cities. Renew. Sustain. Energy Rev. 106, 17–30. https://doi.org/10.1016/j.rser.2019.02.019.
Li, S., Dong, K., Wang, J., Zhang, X., 2015. Long term coupled simulation for ground source heat pump and underground heat exchangers. Energy Build. 106, 13–22. https://doi.org/10.1016/j.enbuild.2015.05.041.
Bernier, M., 2006. Closed-loop heat pump systems. ASHRAE J. 13–19.
Fossa, M., Rolando, D., 2016. Improved Ashrae method for BHE field design at 10 tear horizon. Energy Build. 116, 114–121. https://doi.org/10.1016/j.enbuild.2015.12.051.
Norme Suisse, S.I.A.. Sondes géothermiques. SIA 384/6. Zurich: Société suisse des ingénieurs et des architectes; 2010.
project, G.R.E.T.A., 2017. Catalogue of operational criteria and constraints for shallow geothermal systems in the. Alpine Environ. 4.